

TESTING EVOLUTION OF LFQPOS WITH MASS ACCRETION RATE IN GRS 1915+105 WITH *INSIGHT*–HXMT

HONGHUI LIU¹, LONG JI², COSIMO BAMBI^{1,†}, PANKAJ JAIN³, RANJEEV MISRA⁴, DIVYA RAWAT³, J S YADAV³ AND YUEXIN ZHANG⁵

Draft version March 10, 2021

ABSTRACT

Using the *Insight*–HXMT observations of GRS 1915+105 when it exhibits low frequency quasi-periodic oscillations (QPOs), we measure the evolution of the QPO frequency along with disk inner radius and mass accretion rate. We find a tight positive correlation between the QPO frequency and mass accretion rate. Our results extend the finding of previous work with *AstroSat* to a larger range of accretion rate with independent instruments and observations. Treating the QPO frequency of GRS 1915+105 as the relativistic dynamic frequency of a truncated disk, we are able to confirm the high spin nature of the black hole in GRS 1915+105. We also address the potential of our finding to test general relativity in the future.

Subject headings: accretion, accretion disks — black hole physics — gravitation

1. INTRODUCTION

Quasi-periodic oscillations (QPOs; van der Klis 2005) in the form of narrow peaks in the power spectral density (PSD) are often observed in X-ray binaries (XRBs). The phenomenon is found to have similar characteristics in both neutron star and black hole accreting systems (e.g. Wijnands & van der Klis 1999), suggesting a common physical origin (e.g. accretion/ejection flow).

Over the last three decades, we have accumulated abundant knowledge about the behavior of QPOs in black hole XRBs. Correlation between the QPO frequencies and disk flux in hard state has been found in some systems (Remillard & McClintock 2006; Motta et al. 2011). There is also clear evidence showing positive correlation between the lower frequency break (ν_b) and Low frequency QPOs (LFQPOs) (e.g. Wijnands & van der Klis 1999; Belloni et al. 2002). Another tight correlation between LFQPOs and high frequency QPOs (or broad noise component) is found to exist over a large frequency range (Psaltis et al. 1999). These findings help to put strong constraints on models to explain QPOs.

LFQPOs have frequency roughly in the range 0.05–30 Hz. In black hole systems, LFQPOs can be divided into several types (Type A, B and C; See Casella et al. 2004, 2005). It has been found in some systems that different types of QPOs occur in different stages of the outburst of black hole transients (Motta et al. 2011). Understanding the origin and mechanism of QPOs can give us important hints on both accretion/ejection process and the spacetime property near compact objects. For

instance, Motta et al. (2014) measured the black hole spin of XTE J1550-564 using a simultaneous detection of type-C and high frequency QPOs. There is also attempt to estimate black hole mass assuming that the correlation between LFQPOs and high energy spectrum index scales with mass (Shaposhnikov & Titarchuk 2007).

Models proposed to explain LFQPOs refer mainly to instabilities or geometric effects. For instance, Tagger & Pellat (1999) proposed a model in which accretion-ejection instability (AEI) of a magnetized accretion disk can connect to QPOs observed in XRBs. Stella & Vietri (1998) interpreted the QPOs in low mass XRBs as Lense-Thirring precession of the innermost region of the accretion disk. Also in the frame of Lense-Thirring precession, Ingram et al. (2009) considered the precession of the hot flow inside a truncated disk and were able to explain why the observed maximum frequency is almost constant for all black hole XRBs. These models have been further extended and applied to observation data (Varnière & Tagger 2002; Titarchuk & Fiorito 2004; Cabanac et al. 2010; Ingram & Done 2011; Veledina et al. 2013; Varnière et al. 2012; Karpouzas et al. 2020; Ma et al. 2020). However, we have not reached a unified model that can explain all QPO behaviors.

Recently, Misra et al. (2020) confirmed the high spin of the black hole in GRS 1915+105 using a spectral timing analysis of its X-ray radiation with *AstroSat* (Yadav et al. 2016; Agrawal 2017) data. The authors were able to simultaneously measure the QPO centroid frequency, disk inner radius and mass accretion rate. A correlation between the QPO frequency divided by the accretion rate and inner disk radius was found, which is expected if the QPO frequency is related to the dynamic frequency ($f_{\text{dyn}} = c_s(r)/r$, where c_s is the sound speed) of the standard accretion model. This kind of analysis requires both broadband energy coverage (for precision measurement of disk inner radius) and good timing ability of the instruments. We note that the Chinese X-ray satellite *Hard X-ray Modulation Telescope* (dubbed as *Insight*–HXMT, Zhang et al. (2014)) is also capable of measuring broadband energy spectrum and fast time

¹ Center for Field Theory and Particle Physics and Department of Physics, Fudan University, 200438 Shanghai, China. †E-mail: bambi@fudan.edu.cn

² Institut für Astronomie und Astrophysik, Kepler Center for Astro and Particle Physics, Eberhard Karls Universität, Tübingen, Germany

³ Department of physics, IIT Kanpur, Kanpur, Uttar Pradesh 208016, India

⁴ Inter-University Center for Astronomy and Astrophysics, Ganeshkhind, Pune 411007, India

⁵ Kapteyn Astronomical Institute, University of Groningen, PO BOX 800, Groningen NL-9700 AV, the Netherlands

TABLE 1
Insight-HXMT OBSERVATIONS OF GRS 1915+105 ANALYZED IN THIS PAPER

obsID	Date	Exposure (s)
P0101330005	20180407	1759
P0101330006	20180409	5383
P0101330008	20180411	898
P0101330010	20180413	1399
P0101330011	20180414	3004
P0101330012	20180415	4795
P0101330013	20180416	4489
P0101330016	20180430	3494
P0101330017	20180506	4713
P0101310006	20180527	5043
P0101310007	20180601	6457

Note. Only LE exposures are listed. The observation date is presented in the form of *yyyymmdd*.

variability from XRBs, which offers good opportunity to trace the coevolution of the QPOs and the disk parameters.

In this paper, we present a spectral timing analysis of GRS 1915+105 observed by *Insight*-HXMT. The data reduction procedure is summarized in Section 2. We describe the timing and spectral analysis in Section 3. We show the results in Section 4 and discuss the finding in Section 5.

2. OBSERVATION AND DATA REDUCTION

GRS 1915+105 is a special low mass X-ray binary (LMXB) discovered in 1992 by WATCH (Castro-Tirado et al. 1992). Unlike other black hole LMXBs that spend most time in quiescence, the source has been a persistent system since its discovery. It does not follow the typical Q-shape pattern on the hardness intensity diagram, but exhibits much more complex variability instead (see Belloni et al. 2000; Hannikainen et al. 2003).

Insight-HXMT extensively observed GRS 1915+105 from 2017 to 2020. We went through all available *Insight*-HXMT data of GRS 1915+105 and picked out those observations that show QPO signatures. We checked the lightcurve of each observation and excluded the ones with strong variability (e.g. strong flares or dips). Short exposures on the same day are combined after examining the stability of their lightcurves. The selected observations analyzed in this work are marked in the lightcurve of GRS 1915+105 in Figure 1. Information of these observations are listed in Table 1. We also show the hardness ratio and hardness intensity diagram of GRS 1915+105 since 2009 in Figure 2. We use the nearly daily monitoring data of GRS 1915+105 from MAXI and Swift/BAT to create Figure 2. The count rates from both instruments are first scaled into Crab units and the hardness ratio is defined as the ratio between the scaled MAXI and Swift/BAT count rate.

Insight-HXMT is the first Chinese X-ray telescope, which consists of low-energy, medium-energy and high-

energy detectors covering the broadband energy range of 1–250 keV (Chen et al. 2020; Cao et al. 2020; Liu et al. 2020; Zhang et al. 2020). We extract lightcurves and spectra following the official user guide⁶ and using the software HXMTDAS ver 2.02. The background is estimated by standalone scripts *hebkmap*, *mebkmap* and *lebkmap* (Liao et al. 2020a; Guo et al. 2020; Liao et al. 2020b). We screen good time intervals by considering the recommended criteria, i.e., the elevation angle > 10 degree, the geomagnetic cutoff rigidity > 8 GeV, the pointing offset angle < 0.1 and at least 300 s away from the South Atlantic Anomaly (SAA).

We fit spectral data from *Insight*-HXMT Low Energy X-ray Telescope (LE) in energy range 2–9 keV and Medium Energy X-ray Telescope (ME) in 8–20 keV. The High Energy X-ray Telescope (HE) data is not included because of strong background presence. We have also checked that adding HE data made little difference to the best-fit parameters.

3. DATA ANALYSIS

3.1. Timing analysis

We extract the LE light curve of GRS 1915+105 in the 1–10 keV energy band with a time resolution of 1/128 s. Note that we use data in 2–9 keV for spectral analysis (instead of the 1–10 keV for timing analysis) because of calibration uncertainties of LE. The nominal time resolution of LE is 1 ms (corresponding to the Nyquist frequency of 500 Hz), but we are only interested in LFQPOs below 30 Hz in this study and thus a 1/128 s resolution is enough.

We then use the Python package *Stingray* (Huppenkothen et al. 2019) to calculate the power spectral density (PSD) with a segment size of 64 s. The final PSD is obtained by averaging all 64 s segments and is normalized according to Belloni & Hasinger (1990). We logarithmically rebin the PSD so that each bin size is 1.02 times larger than the previous bin. The PSD is then fitted in XSPEC between 0.1–20 Hz using several Lorentzian components (Belloni et al. 2002). We need at least one narrow Lorentzian for the QPO and one zero-centered Lorentzian to fit broader component. More narrow Lorentzians are sometimes included to model harmonic peaks. All QPOs we detect have quality factor (Q) greater than 4 and detection significance greater than 3σ ⁷. One typical PSD is shown in Figure 3. The QPO frequencies we find for each observation are listed in Table 2. The ME lightcurve in 8–30 keV band has been analyzed in the same way and returns consistent measurements of the QPO frequencies. So we report only the results from LE data in Table 2.

3.2. Spectral analysis

We use XSPEC v12.10.1f (Arnaud 1996) with cross section set to Verner et al. (1996) to analyze spectra of GRS 1915+105. As for element abundances, we test both Anders & Grevesse (1989) and Wilms et al. (2000). We find that the choice of abundances does not influence much the best-fit parameters (except for n_{H}). This

⁶ <http://www.hxmt.cn/SoftDoc/67.jhtml>

⁷ The ratio of Lorentzian norm divided by its 1σ negative error is larger than 3.

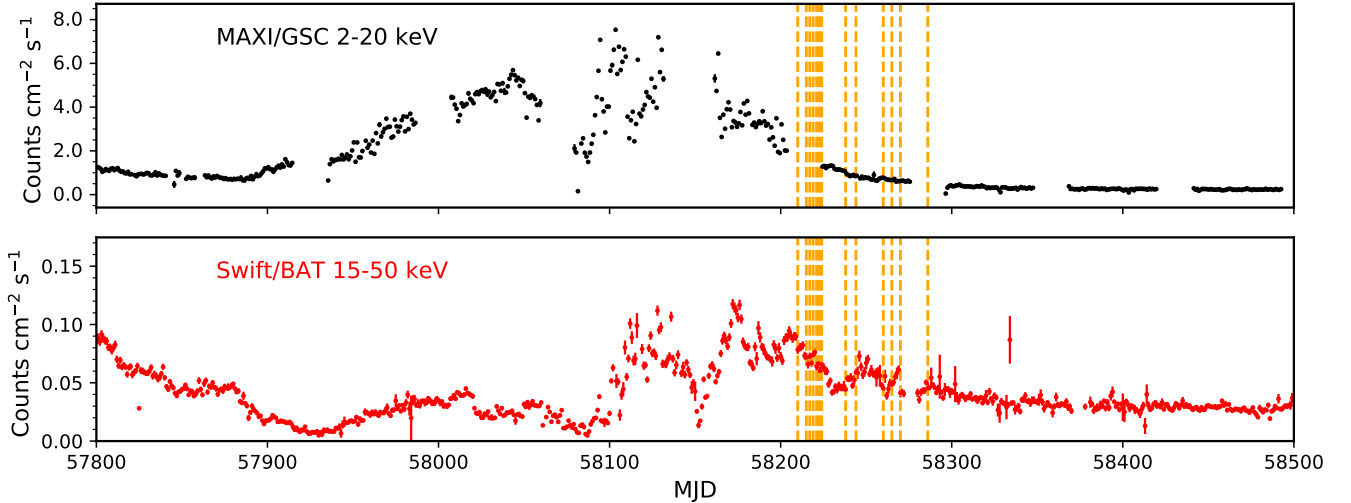


FIG. 1.— MAXI/GSC and Swift/BAT light curves of GRS 1915+105 starting from February 2017. The vertical orange lines mark *Insight*–HXMT observations.

is consistent with what found by Shreeram & Ingram (2020) in the reflection spectrum of GRS 1915+105. We therefore proceed with further analysis using abundances of Wilms et al. (2000), which is more up to date.

The *Insight*–HXMT spectra of GRS 1915+105 are fitted with model $Tbabs \times (simpl \times kerrd + kerrdisk)$. Model *Tbabs* accounts for absorption by Inter-Stellar Medium (ISM) and we set its column density (n_H) to be free during the fitting. *kerrd* (Ebisawa et al. 2003) is included to model the emission from the optically thick accretion disk. The black hole mass, distance and inclination of the accretion disk are set to $12.4 M_\odot$, 8.6 kpc and 60° (Reid et al. 2014), respectively. We also set the spectra hardening factor of *kerrd* to 1.7 (Shimura & Takahara 1995). Comptonization of disk photons is also taken into account by convolving *simpl* (Steiner et al. 2009) with *kerrd*. *kerrdisk* (Brenneman & Reynolds 2006) is used to fit possible blurred fluorescent emission from the accretion disk. The rest frame line energy is fixed at 6.4 keV (Blum et al. 2009). We fix the spin parameter (a_*) to 0.98 and index of the emissivity profile to 1.8 as did by Misra et al. (2020). Leaving these parameters free will not affect much the best-fit values of other parameters. The disk reflection component is always weak (as shown in Figure 3) in the analyzed observations, and the reflection can be well fitted with a simple gaussian at iron band. So we do not consider more sophisticated reflection model (e.g. *relxill* (García et al. 2014)).

We run a Monte Carlo Markov Chain (MCMC) for each spectrum to estimate the uncertainties of free parameters. The XSPEC implementation of MCMC simulation (*Chain* command) using algorithm of Goodman & Weare (2010) is used to generate the chain. We set up 100 walkers to search the parameter space with the first 5000 steps ignored (burn in). The chain lengths differ from case to case, depending on the autocorrelation of each parameter, but we ensure each walker runs 30 times more steps than the longest autocorrelation length. To further test the convergence of the chain, we compare the

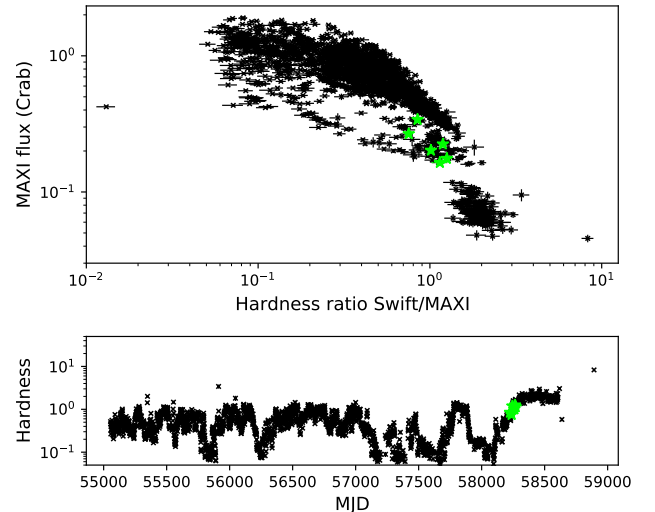


FIG. 2.— Hardness intensity diagram (HID) of GRS 1915+105 from MAXI/GSC (2–20 keV) and Swift/BAT (15–50 keV) monitoring. Hardness ratio is defined as MAXI count rate in Crab units divided by Swift count rate. The *Insight*–HXMT observations analyzed in this work are marked with green stars.

two dimensional distribution for each pair of parameters from the first and second halves of the chain and we find no large difference.

4. RESULTS

The best-fit values and errors extracted from the chains are shown in Table 2. It is interesting to note that although the observations analyzed here spread over a 2-month interval and the source luminosity decreases by a factor of 3, the QPO signature is always clearly detected. It might be due to that the corona-disk geometry does not change much during the interval, since the source hardness remains similar for the analyzed observations (see the bottom panel of Figure 2).

Correlation between the QPO frequency, disk inner radius and accretion rate are shown in Figure 4. We run

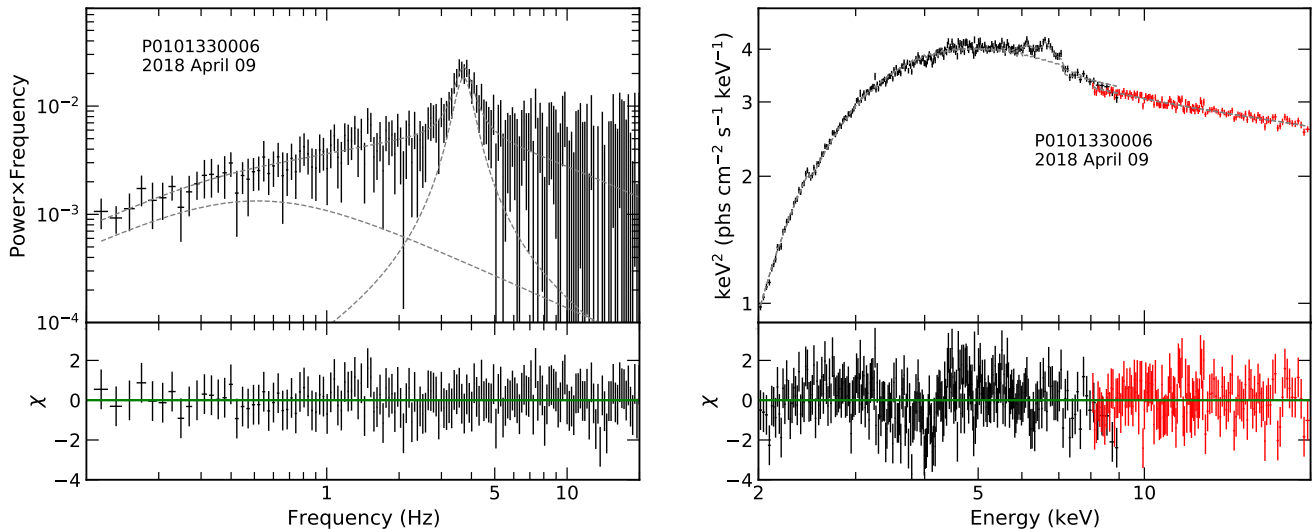


FIG. 3.— Left: The power spectral density (PSD) of GRS 1915+105 observed by *Insight*–HXMT on 2018 April 9 in 1–10 keV. Right: *Insight*–HXMT spectrum of GRS 1915+105 and residuals to the best-fit model. Data from LE and ME are plotted in black and red respectively.

Spearman’s rank correlation analysis and find that the strongest correlation is between the QPO frequency and mass accretion rate (correlation coefficient $\rho = 0.89$ with probability of random results $P < 10^{-3}$). The correlation between QPO frequency and disk inner radius is less significant ($\rho = 0.54$, $P = 8.8\%$). Misra et al. (2020) find a stronger correlation between QPO frequency divided by accretion rate and disk inner radius than the correlation between each pair of these parameters. However, the same correlation we find is weaker than that between the QPO frequency and accretion rate, although the correlation is still strong ($\rho = -0.81$, $P = 0.3\%$). We note that the range of mass accretion rate we explored is much larger than that by Misra et al. (2020). This larger range enables us to find out the direct dependence of QPO frequency on mass accretion rate.

In Misra et al. (2020), the authors identify the QPO frequency of GRS 1915+105 as the dynamic frequency of a truncated disk. The dynamic frequency is defined as the ratio between the sound crossing velocity at the inner disk and the truncation radius ($f_{\text{dyn}} \sim c_s(r)/r$). Assuming a standard relativistic accretion disk (Novikov & Thorne 1973), the dynamic frequency is a function of black hole spin (a_*), mass accretion rate (\dot{M}), truncation radius (R_{in}) and an overall normalization factor (N). Since we can measure the QPO frequency, accretion rate and the truncation radius of GRS 1915+105 with spectral timing analysis, it is possible to infer the spin parameter by fitting the correlation of these parameters (using equation (3) of Misra et al. (2020)).

We fit the relation between QPO frequency divided by accretion rate and disk inner radius using equation (3) of Misra et al. (2020). The fit on *Insight*–HXMT data returns $a_* = 0.99897 \pm 0.00019$ and $N = 0.108 \pm 0.006$. We also try to fit the *Insight*–HXMT and *AstroSat* data simultaneously and we get $a_* = 0.99836 \pm 0.00028$ and $N = 0.121 \pm 0.005$, indicating a rapidly spinning black hole in GRS 1915+105. This measurement of high spin

is consistent with what has been obtained by analyzing the blurred reflection spectra (Blum et al. 2009; Miller et al. 2013; Zhang et al. 2019b) or the thermal spectra (McClintock et al. 2006) of GRS 1915+105. The best-fit curve is shown in Figure 5, as well as the results of Misra et al. (2020).

From Table 2, we see that the column density of **Tbabs** evolves with inner radius and mass accretion rate, which raise the question if the degeneracy of these parameters affects the measurements. In Figure 6, we plot degeneracy of the three parameters for two observations (one has the highest absorption column and the other has the lowest). There is indeed strong correlation between inner radius and mass accretion rate, which is expected since a smaller inner radius can somehow compensate the effect on the spectral shape by a lower accretion rate. This can also explain the degeneracy between column density of the absorption material and accretion rate. However, we find that these parameters are well constrained and we conclude letting $n\text{H}$ free will not include bias on the measurement. We have also checked that holding the column density to be the same for all observations provides unacceptable fits.

5. DISCUSSION AND CONCLUSIONS

With the advantage of broad energy coverage and good time resolution of *Insight*–HXMT, we measure the evolution of LFQPOs signature of GRS 1915+105 along with its mass accretion rate and inner disk radius. Assuming the QPO frequency corresponds to relativistic dynamic frequency of the disk, we are able to confirm the high spin nature of the black hole in GRS 1915+105. Our results extend the previous finding with *AstroSat* (Misra et al. 2020).

In Figure 5, the best-fit curve of Misra et al. (2020) differs substantially from ours for low values of R_{in} . This is due to the lack of data with low values of the disk inner radius in their analysis. At larger values of R_{in} ($R_{\text{in}} > 4r_g$ in Figure 5), our data is systematically lower than the

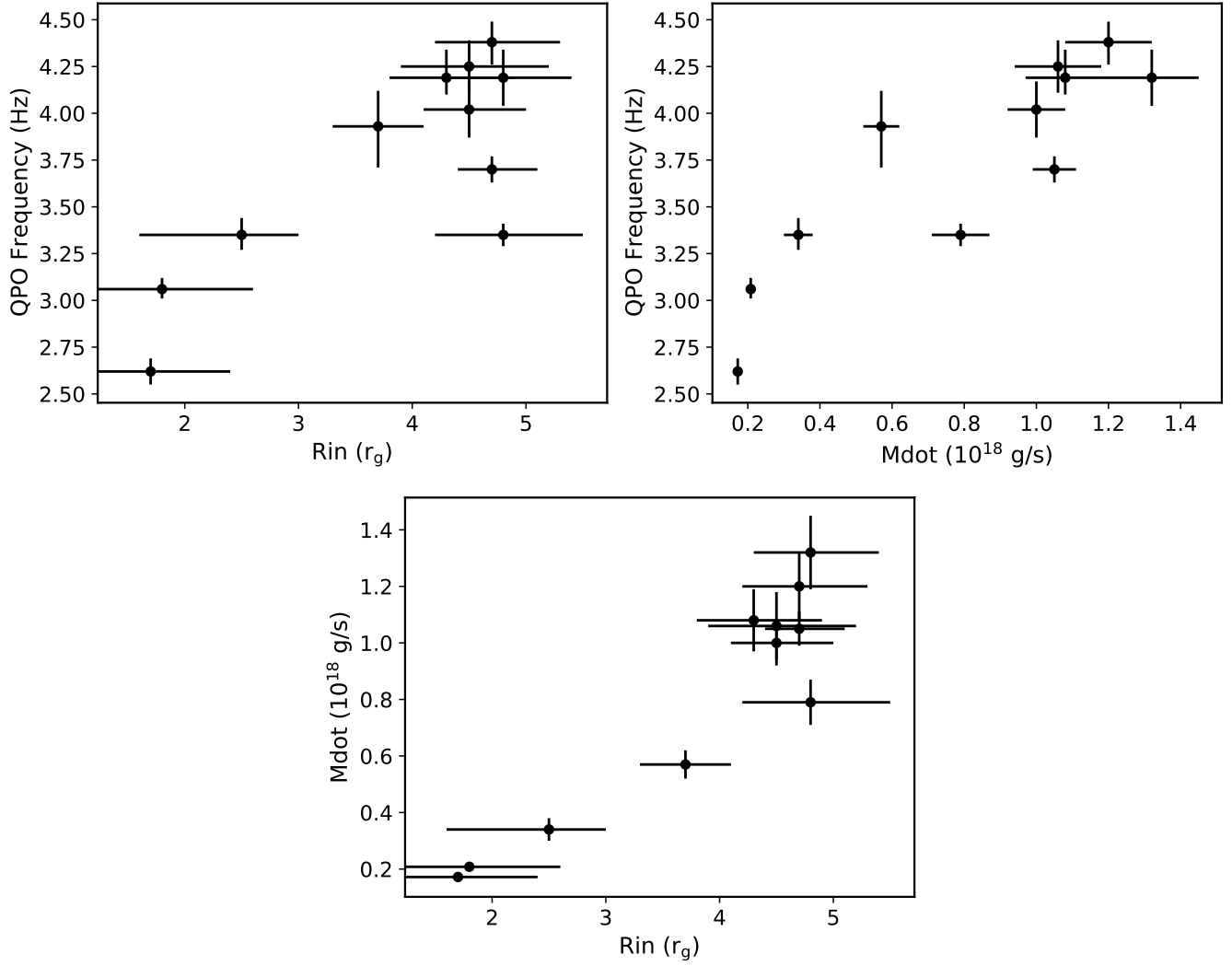


FIG. 4.— QPO frequency v.s. disk inner radius (upper left), QPO frequency v.s. accretion rate (upper right) and accretion rate v.s. disk inner radius (lower).

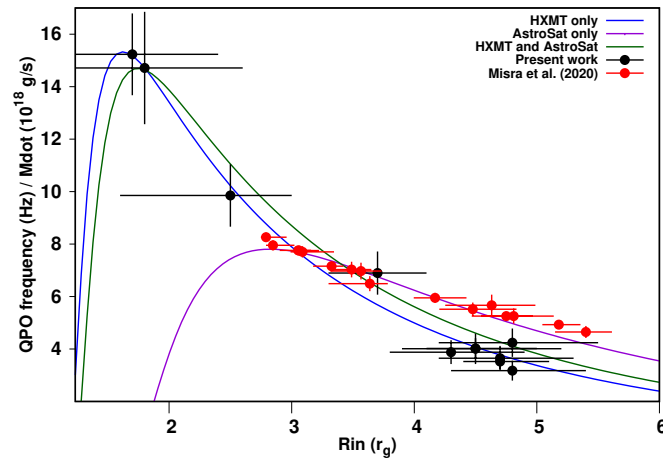


FIG. 5.— QPO frequency divided by accretion rate with disk inner radius. The black and red crosses denote results of this work and of Misra et al. (2020) respectively. The blue curve represents the best-fit of *Insight*-HXMT data only (reduced $\chi^2 = 0.22$) and green curve for fitting both *Insight*-HXMT and *AstroSat* data (reduced $\chi^2 = 0.76$).

TABLE 2
BEST FIT PARAMETERS OF GRS 1915+105

Date ¹	f_a^2	f_u^2	nH (10^{22} cm ⁻²)	Inner Radius (R_g)	QPO frequency (Hz)	Accretion Rate (10^{18} g s ⁻¹)	Γ	Fraction Scatter	χ^2/Dof
20180407	9.8	13.8	$5.66^{+0.21}_{-0.2}$	$4.8^{+0.6}_{-0.5}$	$4.19^{+0.15}_{-0.15}$	$1.32^{+0.15}_{-0.13}$	$2.32^{+0.05}_{-0.05}$	$0.51^{+0.05}_{-0.04}$	436.53/426
20180409	8.4	11.4	$5.27^{+0.12}_{-0.11}$	$4.7^{+0.4}_{-0.3}$	$3.7^{+0.07}_{-0.07}$	$1.05^{+0.08}_{-0.06}$	$2.23^{+0.022}_{-0.022}$	$0.544^{+0.025}_{-0.023}$	845.44/811
20180411	8.5	12.0	$5.61^{+0.24}_{-0.22}$	$4.7^{+0.6}_{-0.5}$	$4.38^{+0.11}_{-0.12}$	$1.2^{+0.15}_{-0.12}$	$2.28^{+0.04}_{-0.04}$	$0.48^{+0.04}_{-0.04}$	341.95/373
20180413	8.3	11.7	$5.6^{+0.2}_{-0.2}$	$4.3^{+0.6}_{-0.5}$	$4.19^{+0.15}_{-0.09}$	$1.08^{+0.12}_{-0.11}$	$2.22^{+0.05}_{-0.06}$	$0.44^{+0.04}_{-0.04}$	329.53/388
20180414	7.5	10.6	$5.56^{+0.16}_{-0.16}$	$4.5^{+0.5}_{-0.4}$	$4.02^{+0.15}_{-0.15}$	$1.0^{+0.09}_{-0.08}$	$2.26^{+0.03}_{-0.04}$	$0.48^{+0.03}_{-0.03}$	608.07/635
20180415	7.9	11.0	$5.78^{+0.25}_{-0.24}$	$4.5^{+0.7}_{-0.6}$	$4.25^{+0.14}_{-0.14}$	$1.06^{+0.15}_{-0.12}$	$2.22^{+0.06}_{-0.06}$	$0.43^{+0.05}_{-0.04}$	301.74/331
20180416	6.7	9.1	$5.1^{+0.19}_{-0.17}$	$4.8^{+0.7}_{-0.6}$	$3.35^{+0.06}_{-0.06}$	$0.79^{+0.1}_{-0.08}$	$2.15^{+0.021}_{-0.022}$	$0.603^{+0.029}_{-0.027}$	833.9/743
20180430	5.2	7.1	$5.06^{+0.17}_{-0.16}$	$3.7^{+0.4}_{-0.4}$	$3.93^{+0.19}_{-0.22}$	$0.57^{+0.06}_{-0.05}$	$2.175^{+0.027}_{-0.027}$	$0.469^{+0.024}_{-0.023}$	589.93/616
20180506	4.7	6.1	$4.35^{+0.18}_{-0.18}$	$2.5^{+0.5}_{-0.9}$	$3.35^{+0.09}_{-0.08}$	$0.34^{+0.04}_{-0.04}$	$2.08^{+0.026}_{-0.023}$	$0.557^{+0.027}_{-0.023}$	708.31/652
20180527	3.5	4.5	$4.3^{+0.17}_{-0.1}$	$1.8^{+0.8}_{-P}$	$3.06^{+0.06}_{-0.05}$	$0.208^{+0.03}_{-0.008}$	$2.064^{+0.02}_{-0.019}$	$0.655^{+0.029}_{-0.027}$	519.54/556
20180601	3.3	4.2	$4.09^{+0.12}_{-0.1}$	$1.7^{+0.7}_{-P}$	$2.62^{+0.07}_{-0.07}$	$0.172^{+0.017}_{-0.006}$	$2.05^{+0.016}_{-0.016}$	$0.79^{+0.03}_{-0.03}$	669.21/621

Note. (1) The observation date is presented in the form of *yyyymmdd*. (2) The absorbed and unabsorbed flux in the 2–10 keV energy band in units 10^{-9} ergs s⁻¹ cm⁻². Uncertainties correspond to the 5th and 95th percentiles from the MCMC samples. The symbol *P* means the errorbar touches the lower (or higher) limit.

AstroSat result. This is why the joint fit (the green line) does not agree well with the data. We note that the dynamic frequency model is a very simple assumption. It might not be able to capture all the factors that drive the variability of LFQPOs of this source. So it is not a surprise that we find some differences between different observations.

It is instructive to see that such a simple model can already roughly explain the behavior of LFQPOs in GRS 1915+105. However, we note that there are still substantial locations in the hardness intensity diagram of the source not explored in this study (see Figure 2). Thus, more observations of GRS 1915+105 by *Insight*–HXMT (and *AstroSat*) are certainly needed to understand the variability of this source.

We note that, although dynamic frequencies of a truncated disk can fit the behavior of LFQPOs in GRS 1915+105, an explanation of how the oscillation is generated is still missing. The Lense-Thirring precession model would predict direct dependence of QPO frequency on disk inner radius (See Ingram et al. 2009; Ingram & Done 2010). However, we find stronger dependence on mass accretion rate. The precession model also predicts anticorrelation between LFQPOs and disk inner radius, which is opposite to what we find (see upper left panel of Figure 4). These discrepancy may suggest that, in this particular case, the precession model is not favored. Note that in the “transition layer model” proposed by Titarchuk & Fiorito (2004), the mass accretion rate can indeed influence LFQPOs frequencies by affecting the γ -parameter (Reynolds number) of the accretion disk. The relation they derived between QPO frequency and γ -parameter (which is proportional to mass accretion rate) is very similar in shape to what we find (see Figure 3 of Titarchuk & Fiorito (2004) and upper right panel of Figure 4). This model might be promising to explain the origin of LFQPOs we find in GRS 1915+105, but further and more detailed investigation is certainly needed.

The lower panel of Figure 4 shows that the inner disk radius tends to decrease when the accretion rate is decreasing (also when the source flux is decreasing). This is counterintuitive as we will expect the opposite for a truncated disk (Done et al. 2007). For typical X-ray transients (e.g. GX 339-4), the disk is believed to be

truncated at large radii at the beginning of the outburst and the inner edge moves to smaller radii as the mass accretion rate increases (see Esin et al. 1997). There are evidences from observation that support this scenario (e.g. Wang-Ji et al. 2018; Chainakun et al. 2020). However, GRS 1915+105 is a source with particular properties (see Belloni et al. 2000). It is a persistent source that spends decades accreting at near-Eddington rate. The accretion dynamics is more complicated if the disk is thick. For instance, in the case of Polish doughnut model (Abramowicz et al. 1978), the inner edge of the disk is determined by the fluid angular momentum. If the fluid angular momentum increases as the mass accretion rate increases, the inner edge will move to larger radii. Moreover, when calculating the evaporation of ion-irradiated disks, Dullemond & Spruit (2005) also find that the inner radius of the cold disk increases with increasing mass accretion rate, which is due to the larger circumference needed to transfer all the matter. These scenarios may explain what we are seeing on GRS 1915+105.

We would also like to address the potential of our finding on testing general relativity in the strong field regime (e.g. Bambi 2017). Once the origin of QPOs is understood, the behavior of QPOs can help to reveal the spacetime properties in the vicinity of the black hole (e.g. Motta et al. 2014). We have been able to test the Kerr hypothesis using the reflection dominated (Zhang et al. 2019b) and thermal dominated (Tripathi et al. 2020) X-ray spectra of black hole X-ray binaries, although systematic uncertainties in modelling can somehow affect the analysis (e.g. Zhang et al. 2019a; Liu et al. 2019; Riaz et al. 2020). GRS 1915+105 is a particularly interesting source, in which we can apply continuum fitting method, reflection spectroscopy and QPO modelling together to constrain possible deviation from Kerr metric. We would expect tight constraint from combination of these techniques. This will be further explored in future work.

Acknowledgments – The work of H.L and C.B. is supported by the Innovation Program of the Shanghai Municipal Education Commission, Grant No. 2019-01-07-00-07-E00035, the National Natural Science Foundation of China (NSFC), Grant No. 11973019, and Fudan University, Grant No. JIH1512604. JL thanks supports from the National Natural Science Foundation of China under Grants No. 11733009, U1938103 and U2038101.

REFERENCES

- Abramowicz, M., Jaroszynski, M., & Sikora, M. 1978, *A&A*, 63, 221
- Agrawal, P. C. 2017, *Journal of Astrophysics and Astronomy*, 38, 27
- Anders, E., & Grevesse, N. 1989, *Geochim. Cosmochim. Acta*, 53, 197
- Arnaud, K. A. 1996, in *Astronomical Society of the Pacific Conference Series*, Vol. 101, *Astronomical Data Analysis Software and Systems V*, ed. G. H. Jacoby & J. Barnes, 17
- Bambi, C. 2017, *Reviews of Modern Physics*, 89, 025001
- Belloni, T., & Hasinger, G. 1990, *A&A*, 227, L33
- Belloni, T., Klein-Wolt, M., Méndez, M., van der Klis, M., & van Paradijs, J. 2000, *A&A*, 355, 271
- Belloni, T., Psaltis, D., & van der Klis, M. 2002, *ApJ*, 572, 392
- Blum, J. L., Miller, J. M., Fabian, A. C., et al. 2009, *ApJ*, 706, 60
- Brenneman, L. W., & Reynolds, C. S. 2006, *ApJ*, 652, 1028
- Cabanac, C., Henri, G., Petrucci, P. O., et al. 2010, *MNRAS*, 404, 738
- Cao, X., Jiang, W., Meng, B., et al. 2020, *Science China Physics, Mechanics, and Astronomy*, 63, 249504
- Casella, P., Belloni, T., Homan, J., & Stella, L. 2004, *A&A*, 426, 587
- Casella, P., Belloni, T., & Stella, L. 2005, *ApJ*, 629, 403
- Castro-Tirado, A. J., Brandt, S., & Lund, N. 1992, *IAU Circ.*, 5590, 2
- Chainakun, P., Luangtip, W., Young, A. J., et al. 2020, *arXiv:2011.04238*
- Chen, Y., Cui, W., Li, W., et al. 2020, *Science China Physics, Mechanics, and Astronomy*, 63, 249505
- Done, C., Gierliński, M., & Kubota, A. 2007, *A&A Rev.*, 15, 1
- Dullemond, C. P. & Spruit, H. C. 2005, *A&A*, 434, 415. doi:10.1051/0004-6361:20042517
- Ebisawa, K., Życki, P., Kubota, A., Mizuno, T., & Watarai, K.-y. 2003, *ApJ*, 597, 780
- Esin, A. A., McClintock, J. E., & Narayan, R. 1997, *ApJ*, 489, 865. doi:10.1086/304829

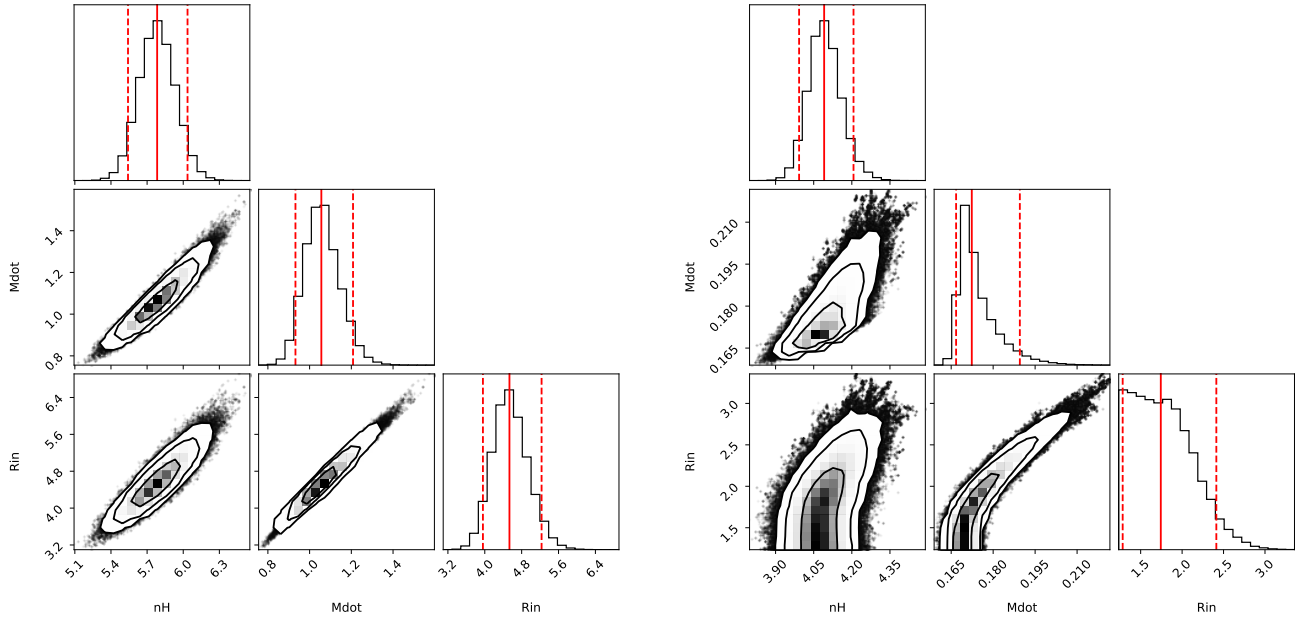


FIG. 6.— Correlation between the column density, disk inner radius and mass accretion rate for observations on 20180415 (left) and 20180601 (right). The red vertical lines denote the 5th, 50th and 95th percentiles for individual parameter.

- García, J., Dauser, T., Lohfink, A., et al. 2014, *ApJ*, 782, 76. doi:10.1088/0004-637X/782/2/76
- Goodman, J., & Weare, J. 2010, *Communications in Applied Mathematics and Computational Science*, 5, 65
- Guo, C.-C., Liao, J.-Y., Zhang, S., et al. 2020, *Journal of High Energy Astrophysics*, 27, 44
- Hannikainen, D. C., Vilhu, O., Rodriguez, J., et al. 2003, *A&A*, 411, L415
- Huppenkothen, D., Bachetti, M., Stevens, A. L., et al. 2019, arXiv e-prints, arXiv:1901.07681
- Ingram, A., & Done, C. 2010, *MNRAS*, 405, 2447
- . 2011, *MNRAS*, 415, 2323
- Ingram, A., Done, C., & Fragile, P. C. 2009, *MNRAS*, 397, L101
- Karpouzas, K., Méndez, M., Ribeiro, E. r. M., et al. 2020, *MNRAS*, 492, 1399
- Liao, J.-Y., Zhang, S., Lu, X.-F., et al. 2020a, *Journal of High Energy Astrophysics*, 27, 14
- Liao, J.-Y., Zhang, S., Chen, Y., et al. 2020b, *Journal of High Energy Astrophysics*, 27, 24
- Liu, C., Zhang, Y., Li, X., et al. 2020, *Science China Physics, Mechanics, and Astronomy*, 63, 249503
- Liu, H., Abdikamalov, A. B., Ayzenberg, D., et al. 2019, *Phys. Rev. D*, 99, 123007
- Ma, X., Tao, L., Zhang, S.-N., et al. 2020, *Nature Astronomy*, arXiv:2009.10607
- McClintock, J. E., Shafee, R., Narayan, R., et al. 2006, *ApJ*, 652, 518
- Miller, J. M., Parker, M. L., Fuerst, F., et al. 2013, *ApJ*, 775, L45
- Misra, R., Rawat, D., Yadav, J. S., & Jain, P. 2020, *ApJ*, 889, L36
- Motta, S., Muñoz-Darias, T., Casella, P., Belloni, T., & Homan, J. 2011, *MNRAS*, 418, 2292
- Motta, S. E., Muñoz-Darias, T., Sanna, A., et al. 2014, *MNRAS*, 439, L65
- Novikov, I. D. & Thorne, K. S. 1973, *Black Holes (Les Astres Occlus)*, 343
- Psaltis, D., Belloni, T., & van der Klis, M. 1999, *ApJ*, 520, 262
- Reid, M. J., McClintock, J. E., Steiner, J. F., et al. 2014, *ApJ*, 796, 2
- Remillard, R. A., & McClintock, J. E. 2006, *ARA&A*, 44, 49
- Riaz, S., Ayzenberg, D., Bambi, C., & Nampalliwar, S. 2020, *MNRAS*, 491, 417
- Shaposhnikov, N., & Titarchuk, L. 2007, *ApJ*, 663, 445
- Shimura, T., & Takahara, F. 1995, *ApJ*, 445, 780
- Shreeram, S., & Ingram, A. 2020, *MNRAS*, 492, 405
- Steiner, J. F., Narayan, R., McClintock, J. E., & Ebisawa, K. 2009, *PASP*, 121, 1279
- Stella, L., & Vietri, M. 1998, *ApJ*, 492, L59
- Tagger, M., & Pellat, R. 1999, *A&A*, 349, 1003
- Titarchuk, L., & Fiorito, R. 2004, *ApJ*, 612, 988
- Tripathi, A., Zhou, M., Abdikamalov, A. B., et al. 2020, *ApJ*, 897, 84
- van der Klis, M. 2005, *Astronomische Nachrichten*, 326, 798
- Varnière, P., & Tagger, M. 2002, *A&A*, 394, 329
- Varnière, P., Tagger, M., & Rodriguez, J. 2012, *A&A*, 545, A40
- Veledina, A., Poutanen, J., & Ingram, A. 2013, *ApJ*, 778, 165
- Verner, D. A., Ferland, G. J., Korista, K. T., & Yakovlev, D. G. 1996, *ApJ*, 465, 487
- Wang-Ji, J., García, J. A., Steiner, J. F., et al. 2018, *ApJ*, 855, 61. doi:10.3847/1538-4357/aaa974
- Wijnands, R., & van der Klis, M. 1999, *ApJ*, 514, 939
- Wilms, J., Allen, A., & McCray, R. 2000, *ApJ*, 542, 914
- Yadav, J. S., Agrawal, P. C., Antia, H. M., et al. 2016, in *Society of Photo-Optical Instrumentation Engineers (SPIE) Conference Series*, Vol. 9905, *Space Telescopes and Instrumentation 2016: Ultraviolet to Gamma Ray*, ed. J.-W. A. den Herder, T. Takahashi, & M. Bautz, 99051D
- Zhang, S., Lu, F. J., Zhang, S. N., & Li, T. P. 2014, in *Society of Photo-Optical Instrumentation Engineers (SPIE) Conference Series*, Vol. 9144, *Space Telescopes and Instrumentation 2014: Ultraviolet to Gamma Ray*, ed. T. Takahashi, J.-W. A. den Herder, & M. Bautz, 914421
- Zhang, S.-N., Li, T., Lu, F., et al. 2020, *Science China Physics, Mechanics, and Astronomy*, 63, 249502
- Zhang, Y., Abdikamalov, A. B., Ayzenberg, D., et al. 2019a, *ApJ*, 875, 41
- Zhang, Y., Abdikamalov, A. B., Ayzenberg, D., Bambi, C., & Nampalliwar, S. 2019b, *ApJ*, 884, 147